Role of TPEN in Amyloid-β$_{25-35}$-Induced Neuronal Damage Correlating with Recovery of Intracellular Zn^{2+} and Intracellular Ca^{2+} Overloading

Wen-bo Chen[1,2] · Yu-xiang Wang[3] · Hong-gang Wang[1] · Di An[1] · Dan Sun[1] · Pan Li[4] · Tao Zhang[1] · Wan-ge Lu[1] · Yan-qiang Liu[1]

Abstract

The overproduction of neurotoxic amyloid-β (Aβ) peptides in the brain is a hallmark of Alzheimer's disease (AD). To determine the role of intracellular zinc ion ($_i$Zn^{2+}) dysregulation in mediating Aβ-related neurotoxicity, this study aimed to investigate whether N, N, N′, N′-tetrakis (2-pyridylmethyl) ethylenediamine (TPEN), a Zn^{2+}-specific chelator, could attenuate Aβ$_{25-35}$-induced neurotoxicity and the underlying mechanism. We used the 3-(4, 5-dimethyl-thiazol-2-yl)-2, 5-diphenyltetrazolium bromide assay to measure the viability of primary hippocampal neurons. We also determined intracellular Zn^{2+} and Ca^{2+} concentrations, mitochondrial and lysosomal functions, and intracellular reactive oxygen species (ROS) content in hippocampal neurons using live-cell confocal imaging. We detected L-type voltage-gated calcium channel currents (L-I$_{Ca}$) in hippocampal neurons using the whole-cell patch-clamp technique. Furthermore, we measured the mRNA expression levels of proteins related to the $_i$Zn^{2+} buffer system (ZnT-3, MT-3) and voltage-gated calcium channels (Cav1.2, Cav1.3) in hippocampal neurons using RT-PCR. The results showed that TPEN attenuated Aβ$_{25-35}$-induced neuronal death, relieved the Aβ$_{25-35}$-induced increase in intracellular Zn^{2+} and Ca^{2+} concentrations; reversed the Aβ$_{25-35}$-induced increase in ROS content, the Aβ$_{25-35}$-induced increase in the L-I$_{Ca}$ peak amplitude at different membrane potentials, the Aβ$_{25-35}$-induced the dysfunction of the mitochondria and lysosomes, and the Aβ$_{25-35}$-induced decrease in ZnT-3 and MT-3 mRNA expressions; and increased the Cav1.2 mRNA expression in the hippocampal neurons. These results suggest that TPEN, the Zn^{2+}-specific chelator, attenuated Aβ$_{25-35}$-induced neuronal damage, correlating with the recovery of intracellular Zn^{2+} and modulation of abnormal Ca^{2+}-related signaling pathways.

Keywords TPEN · Aβ$_{25-35}$ · Zinc ions · Calcium ions signal · ROS · Organelle damage

Introduction

Alzheimer's disease (AD) is a progressive neurodegenerative disease that leads to cognitive impairment accompanied by neuronal dysfunction or death in the elderly [1, 2]. AD patients show atrophy of the cerebral cortex and hippocampus in the brain, which leads to impairment of learning and the ability to form new memories [3]. Amyloid-β (Aβ) aggregates and accumulates in the brain to form amyloid plaques, which are believed to play an important role in the pathogenesis of AD. The neurotoxicity of Aβ can trigger a deleterious cascade of events that accelerate AD progression, including neuronal excitotoxicity damage, intracellular ion dyshomeostasis, oxidative stress, loss of synapses, and cell apoptosis [4–6].

Zinc ions (Zn^{2+}) are essential trace elements in humans and other animals that participate in a variety of physiological

✉ Yan-qiang Liu
liuyanq@nankai.edu.cn; liuyanq2@126.com

1   College of Life Sciences, Nankai University, Tianjin 300071, China

2   School of Basic Medical Science, Henan University, Kaifeng 475004, China

3   Department of Immunology and Pathogenic Biology, School of Basic Medical Sciences, Hebei University of Chinese Medicine, Shijiazhuang 050200, Hebei, China

4   Tianjin Key Laboratory of Cerebral Vascular and Neurodegenerative Diseases, Tianjin Neurosurgery Institute, Department of Neurology, Tianjin Huanhu Hospital Affiliated to Nankai University, Tianjin, China

processes, such as catalytic reactions of enzymes, intracellular signaling, metabolism, differentiation, cellular growth, and neurodevelopment [7]. However, excess free Zn^{2+} has been shown to be neurotoxic and can cause neuronal damage under some pathological conditions [8]. Furthermore, an increase in free Zn^{2+} concentration in the brain or Zn^{2+} dysregulation in neurons is related to the occurrence and development of AD [9, 10]. Several autopsy studies have shown Zn^{2+} increase in the hippocampus and amygdala of AD patients [11]. Excess Zn^{2+} can promote the formation of Aβ oligomers by disrupting the helical structure at the *N*-terminus and inducing β-sheet formation at the C-terminus, along with the formation of intra- and inter-chain salt bridges [12]. Other than exogenous Zn^{2+}, the free Zn^{2+} stored in presynaptic vesicles of some glutamatergic neurons is released into the synaptic cleft along with neurotransmitters in response to synaptic activity, and this could also promote the aggregation of Aβ [13]. Therefore, maintaining Zn^{2+} homeostasis is a potential strategy for AD treatment.

Calcium ions (Ca^{2+}), an important second messenger, are involved in many different neurophysiological functions, including the modulation of membrane excitability and mitochondrial function, synaptic transmission, neuronal intra- and paracellular signaling, reactive oxygen/nitrogen species (ROS/RNS) formation, and apoptosis/necrosis [14, 15]. Ca^{2+} can enter neurons from the extracellular space via membrane-embedded Ca^{2+}-permeable channels, such as voltage-gated calcium channels (VGCCs), non-specific cation channels, *N*-methyl-D-aspartate receptors (NMDAR), and transient receptor potential channels (TRPCs) [16]. In neurons, intracellular Ca^{2+} ($_iCa^{2+}$) is mainly stored in the endoplasmic reticulum (ER) and mitochondria, and cytosolic Ca^{2+} is maintained at low nanomolar concentrations (50–300 nM) when neurons are at rest or having minimal activity [15, 17]. The loss of the ability to handle $_iCa^{2+}$ is one of the central features of aging neurons. The calcium hypothesis suggests that neuronal $_iCa^{2+}$ dysregulation plays an important role in AD [18]. In different experimental models of AD, Ca^{2+} accumulates in neurons, and $_iCa^{2+}$ concentration increases, which is toxic to neurons and triggers subsequent pathological processes that drive AD development [17, 19]. Further evidence suggests that Aβ can increase $_iCa^{2+}$ concentrations via interactions with NMDAR and VGCCs [20, 21]. Collectively, drugs or strategies to correct $_iCa^{2+}$ dysregulation are promising therapeutic approaches for AD treatment.

Mitochondria are organelles in buffering $_iCa^{2+}$ levels by taking up and releasing Ca^{2+}[22]. At synaptic terminals, mitochondria can sequester excess $_iCa^{2+}$ and release Ca^{2+} to prolong their residual levels [23] and is involved in regulating neurotransmission and certain types of short-term synaptic plasticity [24]. Aged and dysfunctional mitochondria are not only defective in their abilities for ATP production and $_iCa^{2+}$ buffering, but can also release harmful ROS that induces neuronal apoptosis [25]. Mitochondrial dysfunction has been suggested as a hallmark of neurodegenerative diseases such as AD, Parkinson's disease (PD), amyotrophic lateral sclerosis, and Huntington's disease (HD) [26]. According to the mitochondrial cascade hypothesis of AD, mitochondrial dysfunction associated with elevated ROS levels accumulates for many years in susceptible patients and leads to synaptic defects, cognitive dysfunction, tau protein and Aβ aggregation, and neuroinflammation at certain time points [27, 28].

Collectively, Aβ-induced deleterious neuronal cascades might be involved in Zn^{2+} and $_iCa^{2+}$ dysregulation, mitochondrial dysfunction, and oxidative stress damage. Our previous studies have shown that N, N, N′, N′-tetrakis-(2-pyridylmethyl)-ethylenediamine (TPEN), a Zn^{2+}-specific chelator with cell membrane permeability, could attenuate soluble Aβ-induced neuronal damage by restoring intracellular Zn^{2+} ($_iZn^{2+}$) concentration and the electrophysiological properties of voltage-gated sodium channels (Nav) and voltage-gated potassium channels (Kv) [29]. However, the detailed mechanisms of increased $_iZn^{2+}$ or abnormal Zn^{2+} homeostasis involved in Aβ neurotoxicity need to be further studied. Therefore, in this study, we first established an in vitro model of AD by exposing primary hippocampal neurons to soluble $Aβ_{25–35}$, and then detected the potential protective effect and possible mechanism of TPEN on $Aβ_{25-35}$-induced neuronal damage through in vitro experiments. Herein, we aimed to elucidate the mechanisms of $_iZn^{2+}$ dysregulation in Aβ-induced neurotoxicity, enrich the pathophysiological theory of AD, and provide a basis for preventing and combating AD using Zn^{2+}-specific chelators.

Materials and Methods

Chemicals and Animals

Dulbecco's modified Eagle medium/F12 + Glutamax™-1, Neurobasal™-A medium, Glutamax™, fetal bovine serum, B27 supplements, antibiotics (penicillin and streptomycin), and 0.25% trypsin–EDTA were purchased from Gibco (Grand Island, NY, USA). Hank's balanced salt solution (HBSS) was purchased from SolarBio (Beijing, China). DNase, cytosine β-D-arabinofuranoside (Ara-C), TPEN, poly-L-lysine, TEA-Cl, 4-AP, and tetrodotoxin (TTX) were purchased from Sigma-Aldrich (MO, USA). We obtained 3-(4, 5-dimethyl-thiazol-2-yl)-2, 5-diphenyltetrazolium bromide (MTT) from Amresco Inc. (Solon, OH, USA). Chemical constructs of Aβ peptides were synthesized by China Peptides Co., Ltd. (Shanghai, China) using the $Aβ_{25–35}$ sequences of human APP. $Aβ_{25–35}$ was dissolved in ddH_2O to prepare a stock solution at a concentration of 100 mM. The concentration of $Aβ_{25–35}$ used in this study was 20 μM. Neonatal Sprague–Dawley rats were purchased from SPF Biotechnology Co., Ltd. (Beijing, China). All experimental protocols were approved by the Ethics Committee of Nankai University.

Primary Hippocampal Neuronal Culture

Primary hippocampal neurons were prepared from early postnatal (postnatal day 0–1) Sprague–Dawley rats (either sex) using protocols described previously [29]. Briefly, the hippocampal tissues were dissected in an ice-cold dissociation buffer (HBSS), minced with forceps, and digested with 0.25% trypsin–EDTA (Invitrogen, UK) at 37 °C for 12 min. The digested tissues were triturated in Dulbecco's modified Eagle medium/F12 (Gibco, UK) medium supplemented with 10% fetal bovine serum (Gibco, UK) and 50 μg/mL DNase (Sigma, USA) using a fire-polished plastic pipette. The cell suspension was centrifuged at $100 \times g$ for 5 min, and the cells were re-suspended in the following plating medium: Dulbecco's modified Eagle medium/F12 medium supplemented with 10% fetal bovine serum, 5 unit/mL penicillin, and 50 μg/mL streptomycin (all from Gibco, UK). The cell suspension was then filtered through a 74-μm screen mesh and was plated into poly L-lysine-coated 96-well plates or 35-mm culture dishes at a density of 120 cells/mm^2 in the plating medium. After 4–6 h, the plating medium was replaced with a maintenance medium, which consisted of Neurobasal-A medium supplemented with 2% B27, 1% Glutamax, 50 μg/mL streptomycin, and 5 unit/mL penicillin (all from Gibco, UK). On day 3, Ara-C (Sigma, USA) was added at a final concentration of 1–5 μM to inhibit glial overgrowth. Cells were cultured in a humidified 5% CO_2 incubator at 37 °C, with half of the maintenance medium replaced every 3 days. Neurons were cultured for 8–12 days in vitro before the experiments.

Experimental Design

The cultured hippocampal neurons were divided into three groups: control, Aβ$_{25-35}$, and Aβ$_{25-35}$ + TPEN. In the Aβ$_{25-35}$ group, hippocampal neurons were treated with Aβ$_{25-35}$ in the maintenance medium at a final concentration of 20 μM for 24 h to establish an in vitro model of AD. According to our previous experimental results [29], the most appropriate concentration of TPEN was 100 nM. In the Aβ$_{25-35}$ + TPEN group, hippocampal neurons were treated with TPEN in the maintenance medium at a final concentration of 100 nmol L^{-1} for 30 min before and during the exposure to Aβ$_{25-35}$.

Measurement of Cell Viability Using the MTT Assay

Cultured neuron viability was determined using the MTT assay. The cells were plated in 96-well plates. Following cell treatment, the maintenance medium was removed, and the cells were incubated with MTT solution (5 mg/mL MTT, prepared in HBSS) at 37 °C for 4 h. Next, the supernatant was discarded, and the formazan particles were dissolved in 100 μL of DMSO. Absorbance was measured at 570 nm using a BIORAD680 plate reader (Thermo, Waltham, MA, USA). The experiments were repeated at least three times, and the results were expressed as the percentage of viable hippocampal neurons compared to the control group.

Single Live–Cell Confocal Imaging

Neurons were seeded in 35-mm glass-bottomed confocal dishes (Nest, China). After the corresponding treatments, neurons were rinsed with HBSS. For Ca^{2+} or Zn^{2+} imaging, neurons were incubated in HBSS containing 2 μM Fluo4-AM (Beyotime Biotechnology, China), 2 μM Fluo-Zin3-AM (Life Technologies, USA), and 0.02% (w/v) pluronic acid (Solarbio) at 37 °C in the dark for 30–60 min. In order to detect the function of the mitochondria and lysosomes, neurons were incubated in HBSS containing 200 nM MitoTracker Red CMXRos, 75 nM LysoTracker Red, or 1 μM Hoechst 33,342 (all from Beyotime Biotechnology) at 37 °C in the dark for 10–25 min. Cellular ROS generation was measured using DCFH-DA (Beyotime Biotechnology, Shanghai, China). Neurons were incubated in HBSS containing 10 μM DCFH-DA at 37 °C in the dark for 20 min. Neurons were then rinsed and kept in HBSS before images were captured. The fluorescence of Fluo4-AM (laser, 488 nm; emission, 512–520 nm), FluoZin3-AM (laser, 488 nm; emission, 516 nm), MitoTracker Red CMXRos (laser, 579 nm; emission, 599 nm), LysoTracker Red (laser, 577 nm; emission, 590 nm), DCFH-DA (laser, 488 nm; emission, 525 nm), and Hoechst 33,342 (laser, 350 nm; emission, 461 nm) was measured with a confocal laser-scanning microscopic system (TCSSP5, Leica, Germany). Image-Pro Plus software was used to analyze the fluorescence intensity of the images.

Whole-Cell Patch-Clamp Recording of Cultured Hippocampal Neurons

Whole-cell patch-clamp recordings were performed to record L-I$_{Ca}$ in primary hippocampal neurons at room temperature (22–25 °C). The recording micropipettes were pulled using a micropipette horizontal puller (P-97, Sutter Instrument Company, USA) from a borosilicate capillary glass. After being filled with the intracellular solution, the pipettes were chosen for the recordings, with the tip resistance ranging from 3 to 5 MΩ. Cultures were mounted on the stage of an inverted microscope (BX51W1, Olympus, Japan) and incubated with the extracellular solution. Hippocampal neurons were patched in whole-cell voltage clamp mode and recorded using a Multiclamp 700B amplifier (Molecular Devices, Foster City, CA, USA). Digidata 1440A (Molecular Devices) was used to digitize the data. pClamp 10.1 software (Molecular Devices) was used for

data acquisition. Recordings were accepted only if the series resistance was less than 20 MΩ and if it did not vary by over 20% throughout the experiment.

To record L-I_{Ca}, the intracellular solution contained 110 mM CsCl, 30 mM TEA-Cl, 10 mM EGTA, 10 mM HEPES, and 3 mM $Na_2ATP·3H_2O$ (pH 7.3 with CsOH), and the extracellular solution contained 110 mM choline chloride, 10 mM $BaCl_2$, 1 mM $MgCl_2·6H_2O$, 10 mM HEPES, 10 mM glucose, 4 mM 4-AP, 20 mM TEA-Cl, and 0.001 mM TTX (pH 7.4 with Tris).

To eliminate the influence of neuronal size, the currents were normalized to the cell membrane capacitance and presented as current densities (pA/pF).

Quantitative Real-Time PCR

Total RNA was extracted from cultured neurons using the TransZol Up Plus RNA Kit (TransGen Biotech, Beijing, China), according to the manufacturer's instructions. The mRNA was reverse-transcribed into cDNA using HiScript® II Q RT SuperMix for qPCR (Vazyme, Nanjing, China). The primer pair sequences used are listed in Table 1. RT-PCR was performed on a RealPlex2 Mastercycler (Eppendorf, Stevenage, UK) using 2×Universal SYBR Green Fast qPCR Mix (ABclonal, Wuhan, China). Cycling conditions were as follows: 95 °C for 3 min and 40 cycles of 95 °C for 5 s, then 60 °C for 30 s. At the end of the cycling process, melting curve analysis was performed on each sample to confirm amplification specificity. β-actin mRNA was used as an endogenous control. All samples were run in triplicate. RT-PCR was repeated at least three times for each gene. Fold changes in the target genes were calculated using the comparative ($2^{-\Delta\Delta CT}$) method [30].

Statistical Analysis

The experimental results were analyzed using Clampft 10.3 (Molecular Devices), Origin 8.5, and SPSS (IBM SPSS Statistics for Windows, Version 20.0. Armonk, NY: IBM Corp.). All data were expressed as mean ± standard error of the mean (SEMs). Statistical significance was assessed by one-way analysis of variance, with significance at the level of $p < 0.05$ and extreme significance at the level of $p < 0.01$.

Results

TPEN Increased the Cell Viability of Hippocampal Neurons Exposed to Aβ$_{25–35}$

The effect of TPEN on the viability of Aβ$_{25–35}$-treated hippocampal neurons was examined using the MTT assay. As shown in Fig. 1, exposure to 20 μM Aβ$_{25–35}$ for 24 h led to significant neuronal death in control neurons (Aβ$_{25–35}$ treatment vs. control: $p < 0.01$). However, Aβ$_{25–35}$-induced neuronal death was markedly attenuated by treatment with 100 nM TPEN, although neuronal death could not be completely prevented (Aβ+TPEN vs. Aβ, $p < 0.01$; Aβ+TPEN vs. control, $p < 0.01$).

TPEN inhibited Aβ$_{25–35}$-induced $_iZn^{2+}$ and $_iCa^{2+}$ concentration increase in hippocampal neurons

To investigate the concentrations of $_iZn^{2+}$ and $_iCa^{2+}$ in primary hippocampal neurons, we used cell-permeant Zn^{2+}- and Ca^{2+}-selective fluorescent indicators, that is, FluoZin-3 and Fluo-4 AM, respectively, to examine the $_iZn^{2+}$ and $_iCa^{2+}$ concentrations in individual hippocampal neurons. Live-cell confocal imaging showed that both FluoZin-3 and Fluo-4 AM fluorescence intensities were significantly increased after Aβ$_{25-35}$ treatment, which indicated that both $_iZn^{2+}$ and $_iCa^{2+}$ concentrations were increased after being treated with Aβ$_{25-35}$ (Figs. 2 and 3); however, TPEN treatment strongly suppressed the Aβ$_{25–35}$-induced $_iZn^{2+}$ and $_iCa^{2+}$ concentration increases (Figs. 2 and 3), especially the $_iZn^{2+}$ concentration, to the point where there was no difference between the Aβ+TPEN and control groups ($p > 0.05$).

TPEN Inhibited Aβ$_{25–35}$-Induced Increase of L-I_{Ca} Density in Hippocampal Neurons

L-type voltage-gated calcium channel currents (L-I_{Ca}) in primary hippocampal neurons were examined using whole-cell patch-clamp recordings. To record L-I_{Ca}, hippocampal neuron potentials were held at -50 mV, and current traces were evoked using a 250-ms constant depolarizing pulse from -60 to $+40$ mV in increments of 10 mV (Fig. 4a). Consequently, Aβ$_{25–35}$ significantly increased the maximum current density of L-I_{Ca} compared to the control (from -17.40 ± 1.08 pA/pF to -27.61 ± 1.75 pA/pF, $p < 0.01$; Fig. 4b). Furthermore, the

Table 1 Primer sequences used in RT-PCR

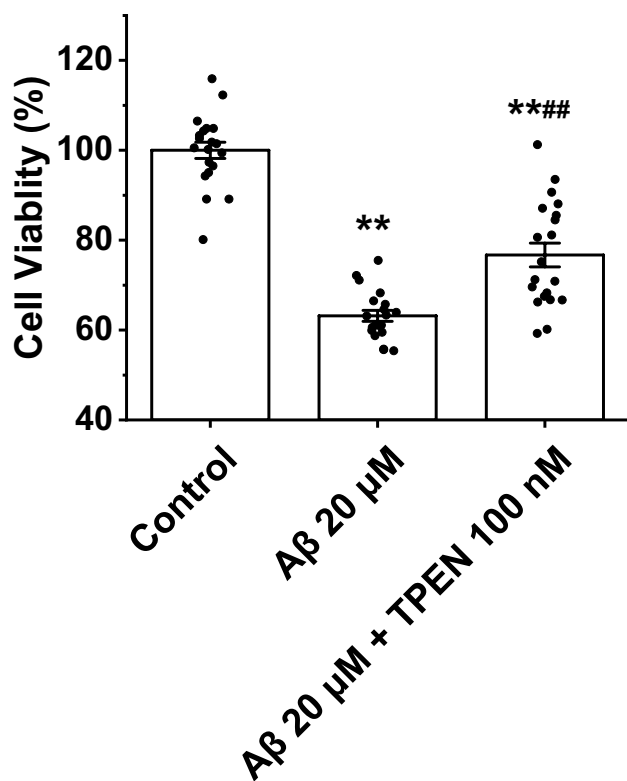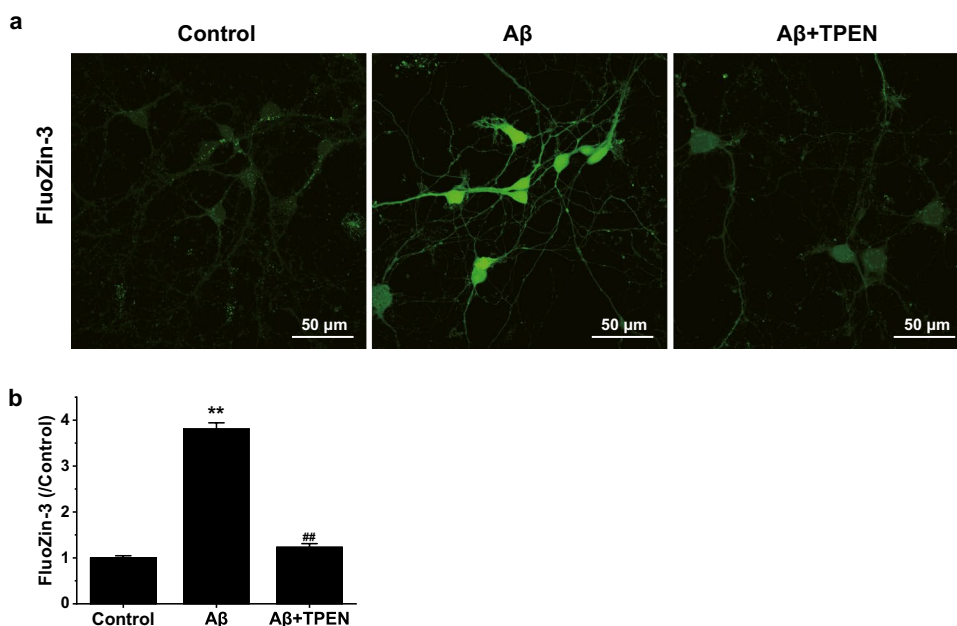| Gene	Gene loci	Forward primer (5′-3′)	Reverse primer (5′-3′)
ZnT-3	NM_001013243.1	GACCAAAGTGTATATGAAGGCAGTG	CAGGAATCGTAGAGGACAAGCA
MT-3	NM_053968.3	CCCTGTCCTACTGGTGGTTC	TTGGCACACTTCTCACATCC
Ca$_V$1.2	NM_012517.2	GGCATCACCAACTTCGACA	TACACCCAGGGCAACTCATA
Ca$_V$1.3	NM_017298.1	TGACATTGGGCCAGAAATCC	GGTGGTATTGGTCTGCTGAA
β-actin	NM_031144.3	CGTTGACATCCGTAAAGACCT	TCAGGAGGAGCAATGATCTTG

Fig. 1 Effects of TPEN on the viability of the hippocampal neurons treated with Aβ$_{25-35}$. The data are presented as means ± SEMs; **$p < 0.01$ versus the control group; ##$p < 0.01$ versus the Aβ group; $n = 20$. Aβ, amyloid-β

L-I$_{Ca}$ increased at different membrane potentials after exposure to Aβ$_{25-35}$, which were visible from the current–voltage (I–V) curves (Fig. 4c), compared to that after exposure to the control ($p < 0.05$). However, TPEN treatment not only completely

reversed the increase in the maximum L-I$_{Ca}$ current density caused by Aβ$_{25-35}$, but also prevented the Aβ$_{25-35}$-induced downward shift of the I-V curves (Aβ+TPEN vs. Aβ, $p < 0.05$; Aβ+TPEN vs. control, $p > 0.05$; Fig. 4b, c).

TPEN Reversed Aβ$_{25-35}$-Induced Changes in the mRNA Expression of Proteins Related to the $_i$Zn^{2+} Buffer System and Ca$_v$ in Hippocampal Neurons

We detected the mRNA expression levels of proteins related to the $_i$Zn^{2+} buffer system (ZnT-3, MT-3) and voltage-gated Ca^{2+} channels (Cav1.2, Cav1.3) in hippocampal neurons using RT-PCR. The results are shown in Fig. 5. After Aβ$_{25-35}$ treatment, the mRNA levels of ZnT-3 and MT-3 were significantly decreased (Aβ vs. control, $p < 0.05$), but the mRNA level of Cav1.2 was significantly increased (Aβ vs. control, $p < 0.05$); however, TPEN treatment completely reversed these Aβ$_{25-35}$-induced changes (Aβ+TPEN vs. Aβ, $p < 0.05$; Aβ+TPEN vs. control, $p > 0.05$), whereas there was no difference in the mRNA level of Cav1.3 among all groups ($p > 0.05$).

TPEN Inhibited Aβ$_{25-35}$-Induced Mitochondrial and Lysosomal Dysfunctions in Hippocampal Neurons

We performed single live-cell confocal imaging to examine mitochondrial and lysosomal functions using MitoTracker Red CMXRos and LysoTracker Red. As shown in Figs. 6 and 7, Aβ$_{25-35}$ treatment noticeably reduced both MitoTracker Red CMXRos and LysoTracker Red fluorescence intensities, suggesting both mitochondrial and lysosomal dysfunctions. However, TPEN treatment completely reversed

Fig. 2 Effects of TPEN on the intracellular Zn^{2+} concentration of the hippocampal neurons treated with Aβ$_{25-35}$. **a** Representative confocal images showing FluoZin-3 (green) staining under the different treatments. The scale bar is 50 μm. **b** Mean fluorescence intensity of FluoZin-3 in the different groups. The data shown in **b** were obtained from three independent experiments, each examining 15–20 neurons for each condition. The data are presented as means ± SEMs; **$p < 0.01$ versus the control group; ##$p < 0.01$ versus the Aβ group. Aβ, amyloid-β

**Fig. 3** Effects of TPEN on the intracellular Ca^{2+} concentration of the hippocampal neurons treated with $A\beta_{25-35}$. **a** Representative confocal images showing Fluo-4 AM (green) staining under the different treatments. The scale bar is 50 μm. **b** Mean fluorescence intensity of Fluo-4 AM in the different groups. The data shown in **b** were obtained from three independent experiments, each examining 15–20 neurons for each condition. The data are presented as means ± SEMs; **$p < 0.01$ versus the control group; ##$p < 0.01$ versus the $A\beta$ group. $A\beta$, amyloid-β
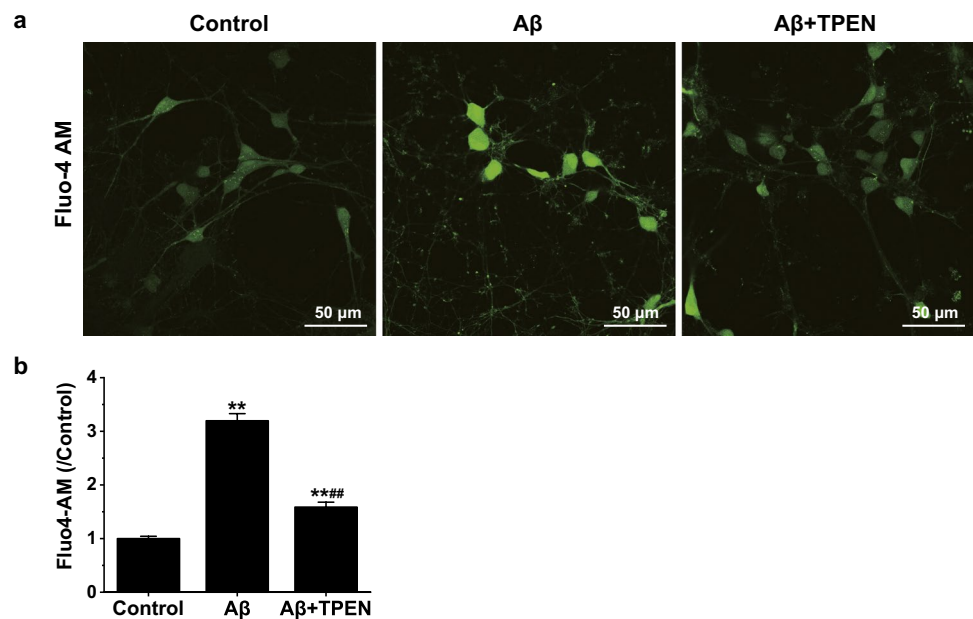
Fig. 4 Effects of TPEN on the amplitude properties of L-I_{Ca} in the hippocampal neurons treated with $A\beta_{25-35}$. **a** Typical example of L-I_{Ca} traces obtained in the hippocampal neurons (left) and record protocol (right). **b** Maximum current density of L-I_{Ca} in the different treatments. **c** Current–voltage (I-V) curves of L-I_{Ca} in the different treatments. The data are presented as means ± SEMs; *$p < 0.05$ and **$p < 0.01$ versus the control group; #$p < 0.05$ and ##$p < 0.01$ versus the $A\beta$ group; $n = 8$ for the control group; $n = 12$ for the $A\beta$ group; $n = 14$ for the $A\beta$ + TPEN group. $A\beta$, amyloid-β; L-I_{Ca}, L-type voltage-gated Ca^{2+} channel current
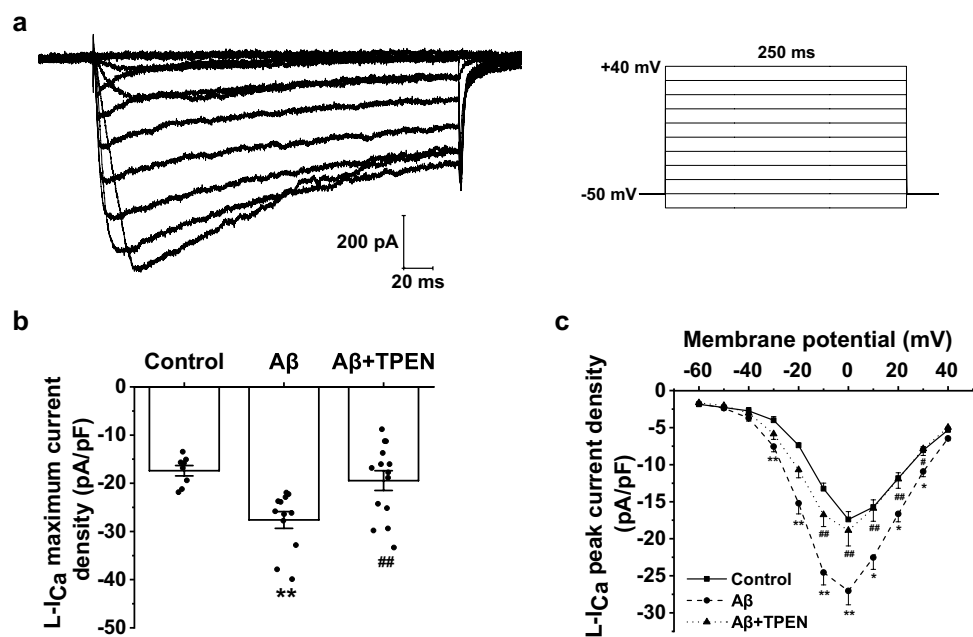
$A\beta_{25-35}$-induced effects ($A\beta$ + TPEN vs. $A\beta$, $p < 0.01$; $A\beta$ + TPEN vs. control, $p > 0.05$).

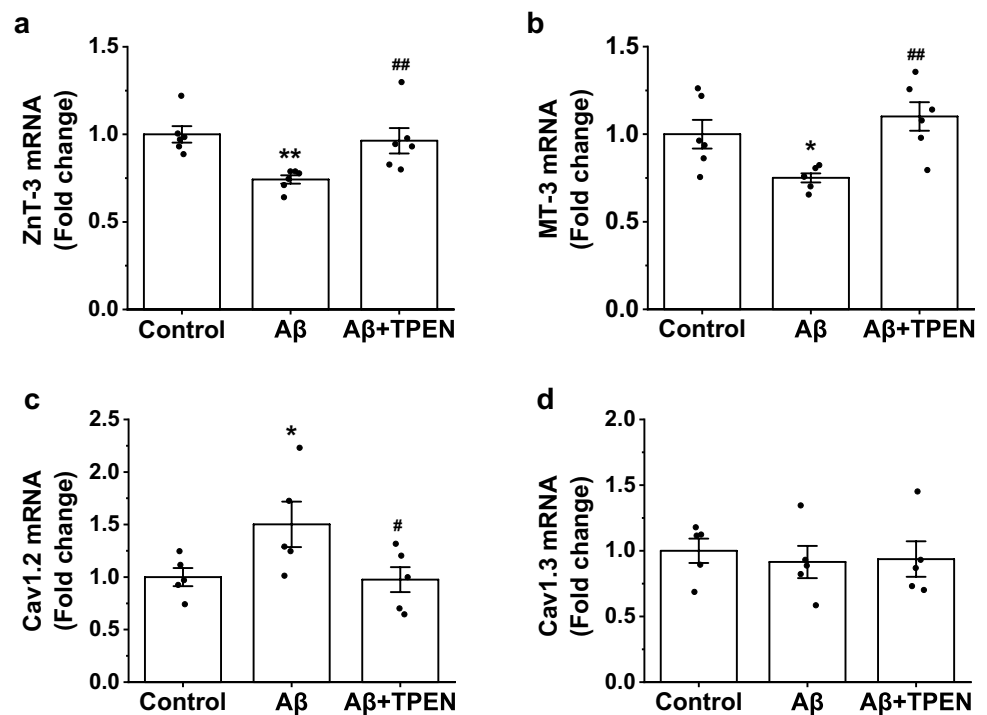## TPEN Inhibited $A\beta_{25-35}$-Induced Cellular ROS Increase in Hippocampal Neurons

The levels of ROS in hippocampal neurons were detected using a DCFH-DA fluorescent probe. Figure 8 shows that $A\beta_{25-35}$ treatment increased the fluorescence intensity of DCFH-DA, which was abolished by TPEN treatment. These

results indicate that TPEN inhibited the $A\beta_{25-35}$-induced increase in cellular ROS in hippocampal neurons.

Discussion

This study showed that TPEN attenuated $A\beta_{25-35}$-induced neuronal death, alleviated $A\beta_{25-35}$-induced increase in $_iZn^{2+}$ and $_iCa^{2+}$ concentrations, reversed the $A\beta_{25-35}$-induced increase in the peak amplitudes of L-I_{Ca} at different

Fig. 5 Effects of TPEN on the mRNA expression of ZnT-3, MT-3, Cav1.2, and Cav1.3 in the hippocampal neurons treated with Aβ$_{25-35}$. **a** Quantification of ZnT-3 mRNA levels. **b** Quantification of MT-3 mRNA levels. **c** Quantification of Cav1.2 mRNA levels. **d** Quantification of Cav1.3 mRNA levels. β-actin was used as an internal control. The data are presented as means ± SEMs; *$p < 0.05$ and **$p < 0.01$ versus the control group; #$p < 0.05$ and ##$p < 0.01$ versus the Aβ group; $n = 5$ or 6; Aβ, amyloid-β

membrane potentials, inhibited Aβ$_{25-35}$-induced mitochondrial and lysosomal dysfunctions, and suppressed the Aβ$_{25-35}$-induced increase in intracellular ROS level. These results suggest that Aβ$_{25-35}$-induced neuronal damage correlates with $_i$Zn^{2+} and $_i$Ca^{2+} dysregulation.

Under physiological conditions, the basal level of extracellular Zn^{2+} is in the low nanomolar (~ 10 nM) range in the hippocampus, which increases with age [31, 32]. Extracellular Zn^{2+} is mainly released from zincergic terminals during synaptic activity, which can interact with postsynaptic-related receptors and ion channels (NMDAR, α-amino-3-hydroxy-5-methyl-4-isoxazole propionic acid receptors (AMPAR), γ-aminobutyric acid (GABA) receptors, glycine receptors, and VGCCs), thus mediating the neuronal excitability and synaptic plasticity [33, 34]. The basal level of $_i$Zn^{2+} is estimated to be less than 1 nM (~ 100 pM), and the body is more sensitive to changes in $_i$Zn^{2+} than to that of extracellular Zn^{2+} [35]. Excess $_i$Zn^{2+} becomes neurotoxic, stimulating neurons to generate ROS and triggering oxidative stress, which eventually leads to cell death [36]. When the Aβ concentration in the extracellular compartment exceeds 100 pM, Aβ can rapidly bind to extracellular Zn^{2+} with high affinity through its histidine residues or carboxyl groups (His6, His13, His14, and AsP1), inducing the formation of Zn-Aβ complexes [37], and rapidly incorporated into neurons to form Zn^{2+}-permeable ion channels [38]. Moreover, free Zn^{2+} can be released from Zn-Aβ oligomers, resulting in increased intracellular Zn^{2+} and Aβ concentrations and inducing neuronal death and cognitive decline [39]. Since there is an age-related increase in extracellular Zn^{2+}

concentration, Aβ-induced $_i$Zn^{2+} neurotoxicity accelerates with aging [38]. In addition, in vivo experiments showed that extracellular Zn^{2+} is essential for Aβ-induced cognitive decline [37]. Furthermore, extracellular Zn^{2+} can also enter cells via Ca^{2+}- and Zn^{2+}-permeable VGCCs, NMDAR, and GluR2-deficient AMPA receptors [40]. Excess influx of extracellular Zn^{2+} is more likely to induce glutamate excitotoxicity than the influx of extracellular Ca^{2+} because the $_i$Zn^{2+} concentration (~ 100 pM) is much lower than the $_i$Ca^{2+} concentration (~ 300 nM) but has higher neurotoxicity [41–43]. Similar to our previous results [29], the present experiment also showed a decrease in neuronal viability and an increase in $_i$Zn^{2+} concentration after exposure to 20 μM Aβ$_{25-35}$ for 24 h, whereas TPEN pretreatment markedly attenuated Aβ$_{25-35}$-induced neuronal death and reversed the Aβ$_{25-35}$-induced $_i$Zn^{2+} concentration increase. These results suggest that $_i$Zn^{2+} dysregulation mediates the neurotoxicity of Aβ$_{25-35}$. Additionally, systemic and cellular Zn^{2+} homeostasis in mammals is usually regulated by the expression and action of $_i$Zn^{2+}-buffering systems, including zinc transporters (ZnTs), metallothioneins (MTs), and Zrt, Irt-related proteins (ZIPs) [44]. Zinc transporter 3 (ZnT-3) is mainly expressed in the cerebral cortex and hippocampus and is responsible for the transport of cytoplasmic Zn^{2+} into presynaptic vesicles [45]. Similarly, metallothionein 3 (MT-3) is principally expressed in the zincergic neurons. As an intracellular Zn^{2+} reservoir, MT-3 is to bind cytoplasmic Zn^{2+} with high affinity and releases Zn^{2+} when needed [46]. Both ZnT-3 and MT-3 are helpful for $_i$Zn^{2+} homeostasis in the brain. However, multiple studies have shown

Fig. 6 Effects of TPEN on the mitochondrial membrane potential of the hippocampal neurons treated with $A\beta_{25-35}$. **a** Representative confocal images showing MitoTracker Red CMXRos staining under the different treatments. The scale bar is 10 μm. **b** Mean fluorescence intensity of MitoTracker Red CMXRos in the different groups. The data shown in **b** were obtained from three independent experiments, each examining 15–20 neurons for each condition. The data are presented as means ± SEMs; **$p < 0.01$ versus the control group; ##$p < 0.01$ versus the Aβ group. Aβ, amyloid-β
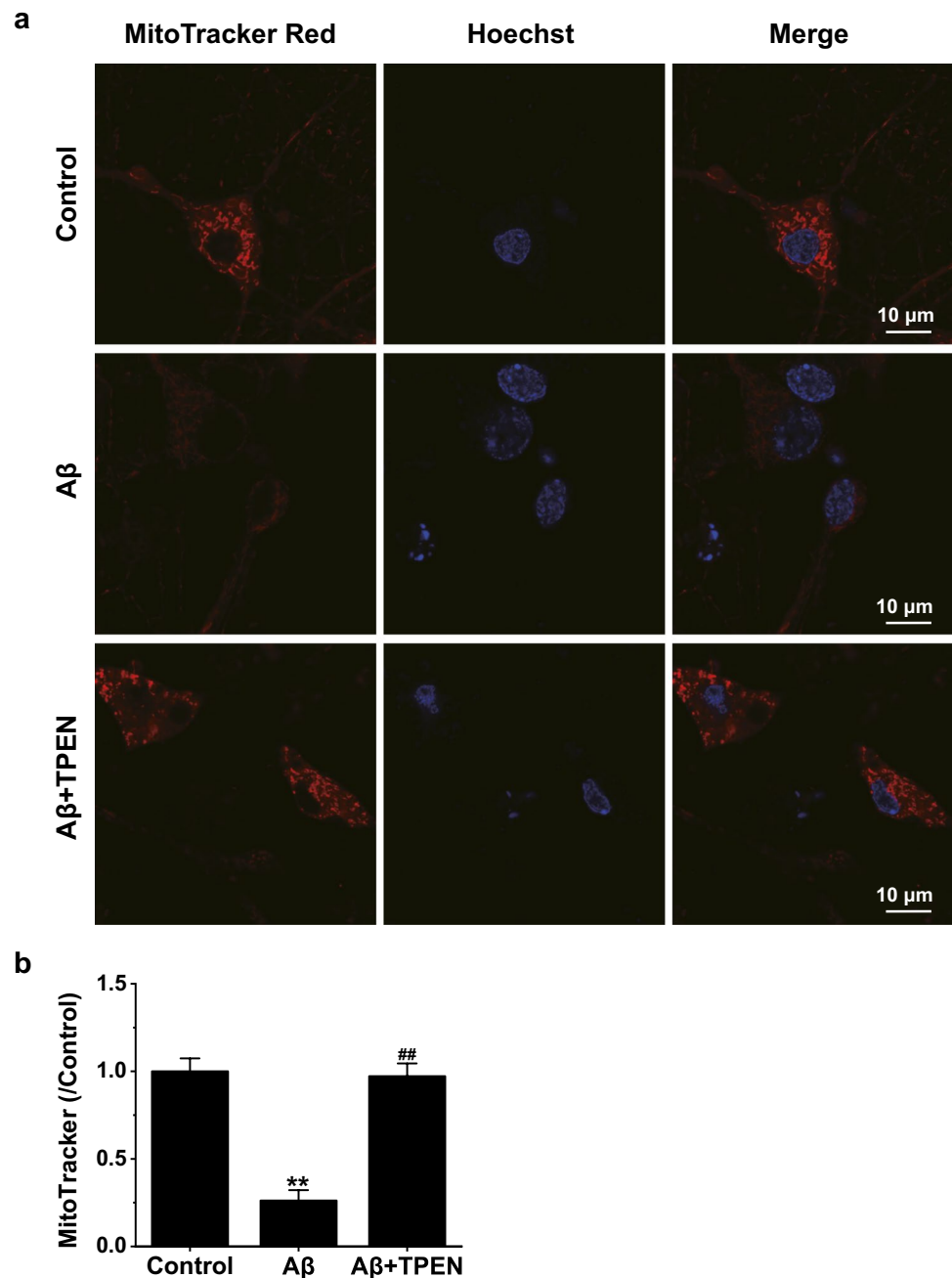
that AD development is accompanied by decreased expression of ZnT-3 and MT-3 [47, 48]. Furthermore, lysosomal dysfunction was observed in MT-3 knockdown astrocytes, consistent with the reduced autophagy observed during AD [49]. Our RT-PCR results showed that $A\beta_{25-35}$ significantly decreased ZnT-3 and MT-3 mRNA levels in hippocampal neurons, whereas TPEN completely reversed these changes. These results suggest that Aβ can induce $_iZn^{2+}$ increase by reducing the mRNA expression levels of MT-3 and ZnT-3 in hippocampal neurons. Furthermore, TPEN partially counteracted Aβ-induced neuronal damage by restoring $_iZn^{2+}$

homeostasis, suggesting that specific Zn^{2+} chelators have potential therapeutic value against AD.

Presenilin, Aβ oligomers, and hyperphosphorylated tau can cause $_iCa^{2+}$ dyshomeostasis [50], which is involved in numerous molecular mechanisms, including increased Ca^{2+} influx by hyperactivated NMDAR and VGCCs, and promoting Ca^{2+} release from the ER by increasing inositol 1,4,5-trisphosphate receptors (IP3R) and ryanodine receptors (RYR) activities [51, 52]. Excessive Ca^{2+} influx can trigger multiple deleterious events including increased ROS, metabolic derangement, excessive inflammation,

Fig. 7 Effects of TPEN on the lysosomal function of the hippocampal neurons treated with $A\beta_{25-35}$. **a** Representative confocal images showing LysoTracker Red staining under the different treatments. The scale bar is 25 μm. **b** Mean fluorescence intensity of LysoTracker Red in the different groups. The data shown in **b** were obtained from three independent experiments, each examining 15–20 neurons for each condition. The data are presented as means ± SEMs; **$p < 0.01$ versus the control group; ##$p < 0.01$ versus the Aβ group. Aβ, amyloid-β
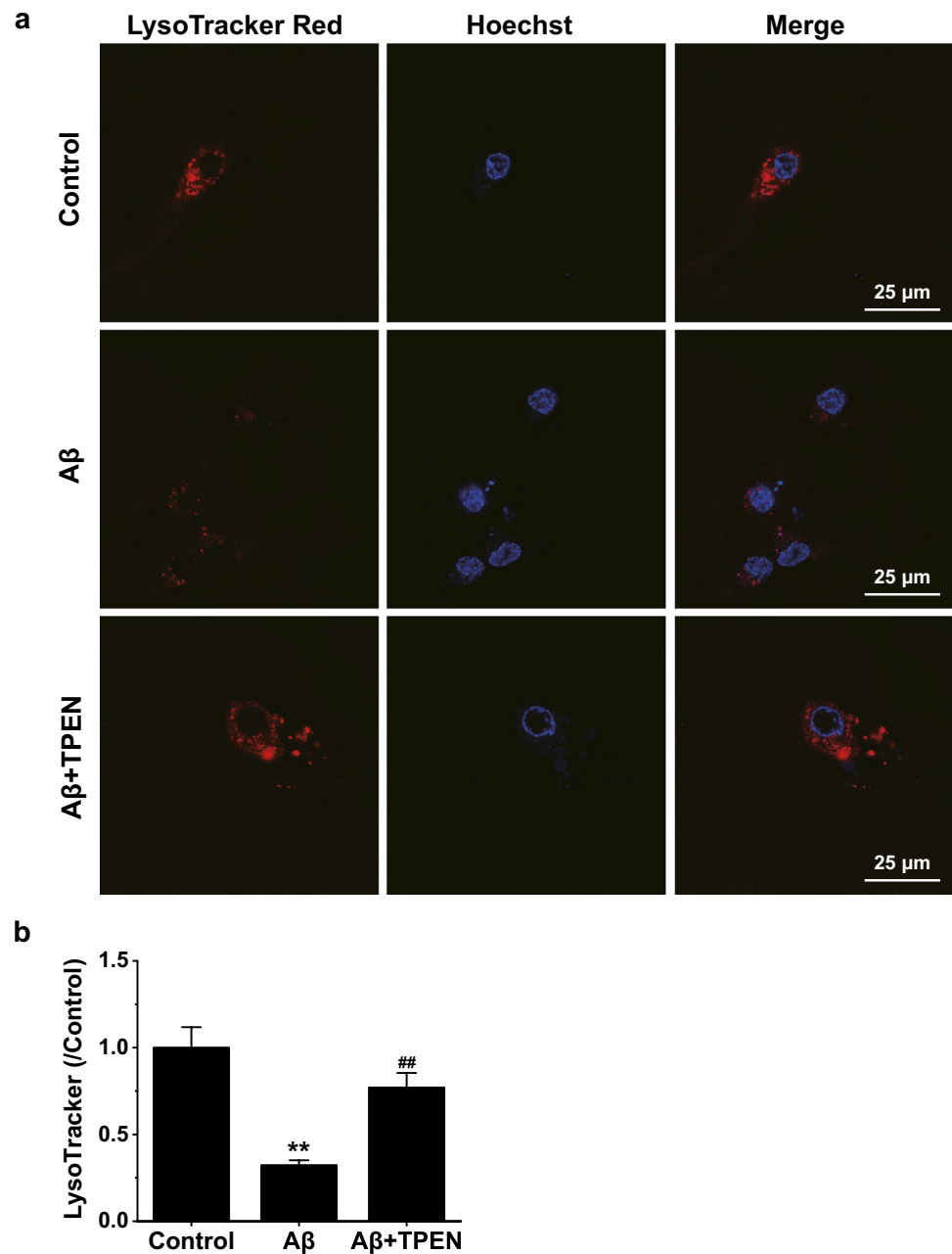
excitotoxicity, mitochondrial dysfunction, and impaired autophagy, all prominent features of AD pathogenesis [16, 19, 53]. Therefore, restoration and maintenance of $_iCa^{2+}$ homeostasis are helpful for the prevention and treatment of AD. In the VGCCs family, L-type voltage-gated calcium channels (LTCCs) can regulate neuronal synaptic plasticity and neuronal excitability by gating Ca^{2+} influx in response to membrane depolarization [54]. There are four known LTCCs ($Ca_v1.1$—$Ca_v1.4$), but only two, $Ca_V1.2$ and $Ca_V1.3$, are highly expressed in the brain [55]. There is increasing evidence of enhanced LTCCs activity in neurodegenerative diseases, such as PD and AD [56, 57]. The enhanced LTCCs activities on neurons are linked to altered mitochondrial function, with detrimental effects most commonly attributed to mitochondrial Ca^{2+} overload [58]. Moreover, LTCC antagonists as potential drugs may prevent the development of dementia [59]. In this study, $A\beta_{25-35}$ significantly increased the $_iCa^{2+}$ concentration in hippocampal neurons and upregulated the expression levels of $Ca_v1.2$ mRNA, which could contribute to the over-activation of LTCCs. Patch-clamp data showed that $A\beta_{25-35}$ markedly increased the maximum current density of L-I_{Ca} and elevated L-I_{Ca} at different membrane potentials, resulting in increased Ca^{2+} influx and increased neuronal excitability. However, TPEN

Fig. 8 Effects of TPEN on the level of ROS in the hippocampal neurons treated with $A\beta_{25-35}$. **a** Representative confocal images showing DCFH (green) staining under the different treatments. The scale bar is 25 μm. **b** Mean fluorescence intensity of DCFH (green) in the different groups. The data shown in **b** were obtained from three independent experiments, each examining 15–20 neurons for each condition. The data are presented as means ± SEMs; $**p < 0.01$ versus the control group; $\#\#p < 0.01$ versus the $A\beta$ group. $A\beta$, amyloid-β
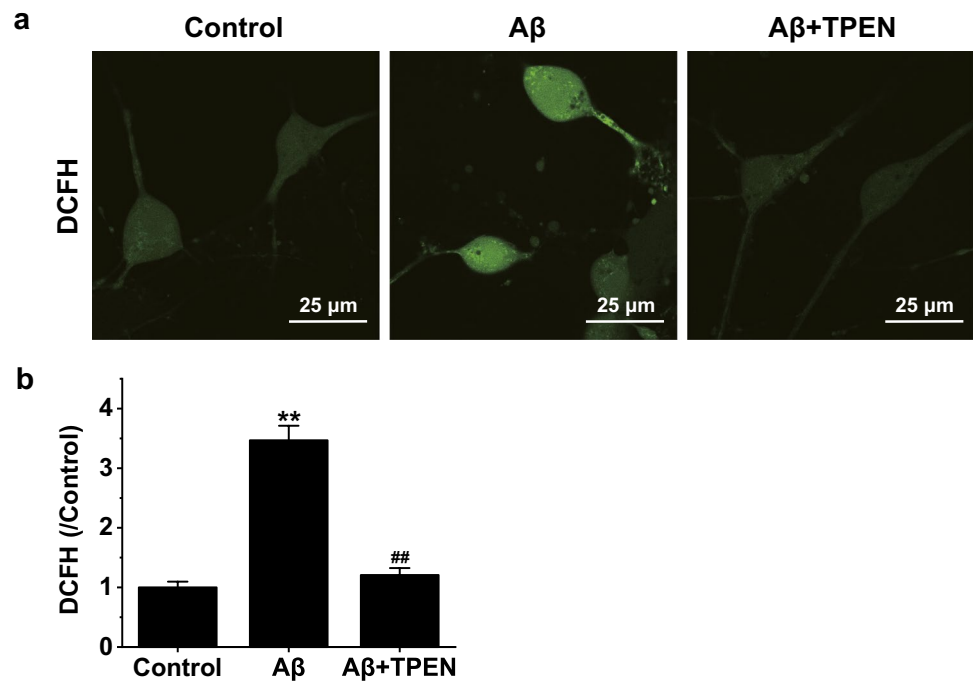
attenuated the $A\beta_{25-35}$-induced $_iCa^{2+}$ concentration increase and reversed the changes in the electrophysiological properties of L-I_{Ca} as well as the $Ca_v1.2$ mRNA expression levels caused by $A\beta_{25-35}$, which suggest that $A\beta_{25-35}$-induced $_iZn^{2+}$ dysregulation mediated the increase in $_iCa^{2+}$ concentration in hippocampal neurons. We have previously shown that $A\beta_{25-35}$-induced increase in $_iZn^{2+}$ concentration had a significant inhibitory effect on voltage-gated K^+ currents in hippocampal neurons [29]. Notably, several studies have shown that blockade of K^+ channels can increase Ca^{2+} influx and lead to $_iCa^{2+}$ accumulation [60, 61]. Therefore, an imbalance in the homeostasis of $_iZn^{2+}$ may lead to $_iCa^{2+}$ increase by inhibiting K^+ channels. Moreover, high concentrations of Zn^{2+} in the cytoplasm can activate RYR and promote Ca^{2+} release from the ER into the cytoplasm, leading to an increase in $_iCa^{2+}$ concentration, which eventually causes neuronal excitotoxic damage [62]. This may also explain the simultaneous dysregulation of $_iZn^{2+}$ and $_iCa^{2+}$ under pathological conditions; however, the specific mechanism involved needs to be further studied.

ROS are primarily produced in the mitochondria as physiological byproducts of various cellular processes and are normally detoxified by enzymes and antioxidants to help maintain neuronal homeostasis [10]. However, mitochondrial dysfunction can lead to excessive ROS production, triggering a state of oxidative stress that can lead to neuronal death. Furthermore, ROS can also contribute to mitochondrial dysfunction either indirectly through the initiation of toxic signaling cascades that target mitochondria or through direct damage to mitochondrial DNA [63]. Notably, ROS

generation is closely related to $_iZn^{2+}$. Mitochondrial Zn^{2+} overload inhibits the mitochondrial electron transport chain and reduces mitochondrial membrane potential, resulting in increased ROS production and decreased cellular ATP levels [64]. Excess $_iZn^{2+}$ also activates other intracellular generators of injurious oxidants, such as lipoxygenases, NADPH oxidases, peroxisomes, and nitric oxide synthases, and promotes the production of neurotoxic peroxynitrite (ONOO$-$), leading to oxidative stress [65]. Interestingly, oxidative stress can promote MT-3 to release additional free Zn^{2+} into the cytoplasm, further exacerbating the increase in $_iZn^{2+}$ concentration [10]. In this study, single live-cell imaging showed that $A\beta_{25-35}$ markedly impaired mitochondrial and lysosomal functions and increased intracellular ROS levels, whereas TPEN significantly inhibited the damages of mitochondrial and lysosomal functions caused by $A\beta_{25-35}$, and reduced intracellular ROS levels. The above statements also showed that $A\beta_{25-35}$ significantly increased both the $_iCa^{2+}$ concentration and intracellular ROS levels in hippocampal neurons, indicating an interlinkage between Ca^{2+} and ROS production. Indeed, accumulating evidence suggests that increased $_iCa^{2+}$ levels may lead to ROS accumulation because of $A\beta$ induction [66, 67]. However, the interactions between Ca^{2+} and ROS signaling systems can be stimulatory or inhibitory, depending on the type of target proteins, ROS species, dose, and exposure time [68]. Therefore, it needs more evidences to clarify the interactions between Ca^{2+} and ROS signaling systems and the condition of causing interaction.
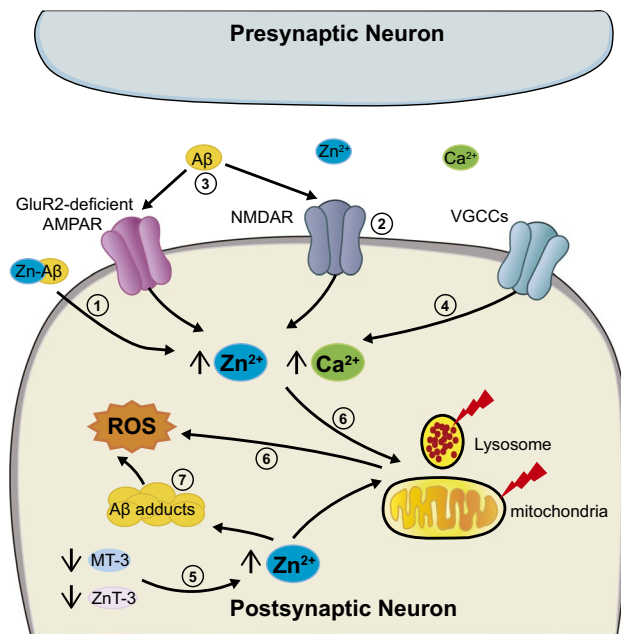
Fig. 9 Synergistic contribution of Aβ, $_iZn^{2+}$ and $_iCa^{2+}$ dysregulation, oxidative stress, and excitotoxicity in AD. The pictogram summarizes the synergistic interaction between AD-related molecular changes, and the cation dysregulation triggered by altered glutamatergic neurotransmission. Accompanying the uptake of the Zn-Aβ complexes into neurons, excess free $_iZn^{2+}$ is released from the Zn-Aβ complexes (1). Extracellular Zn^{2+} and Ca^{2+} can enter cells via VGCCs, NMDAR, and GluR2-deficient AMPAR (2). Aβ adducts can also directly activate NMDAR and GluR2-deficient AMPAR, further promoting the glutamatergic overdrive, inducing $_iZn^{2+}$ and $_iCa^{2+}$ accumulation (3). LTCC overactivation promotes $_iCa^{2+}$ accumulation, increases neuronal excitability, and triggers mitochondrial Ca^{2+} overload (4). The diminished capacity of the iZn^{2+}-buffering system (MT-3, ZnT-3) also contributes to Aβ-induced $_iZn^{2+}$ increase (5). The accumulation of excess $_iZn^{2+}$ is potent neurotoxic and acts synergistically with $_iCa^{2+}$, further promoting mitochondrial and lysosomal dysfunction, ROS generation, and the release of apoptotic molecules (6). Excessive $_iZn^{2+}$ rises may also trigger intraneuronal Aβ aggregation (7). Aβ adducts may further contribute to organelle impairment and ROS production (7). All these processes, set in motion at the level of synaptic spines, may be the primum movens of synaptic dysfunction and neuronal death

Excess $_iZn^{2+}$ is closely associated with lysosomal dysfunction. As acidic organelles containing hydrolase enzymes, lysosomes are indispensable for autophagy, which delivers unnecessary cellular materials to lysosomes for degradation [69]. Decreased autophagy is a distinguishing feature of AD. In APP/PS1-expressing Chinese hamster ovary cells, clioquinol, a Zn^{2+} ionophore, not only attenuated the accumulation of $Aβ_{1-42}$, but also protected cells by overcoming autophagy arrest induced by chloroquine, suggesting that the accumulation of Zn^{2+} in lysosomes was related to Aβ aggregation [70]. Moreover, it has been suggested that cell death may be due to oxidative stress-induced accumulation of Zn^{2+} and Aβ within lysosomes, leading to

lysosomal membrane permeabilization and the subsequent release of Zn^{2+}, Aβ, and other toxic molecules into the cytosol [10, 71]. Taken together, these observations suggest that Aβ-induced $_iZn^{2+}$ increase can trigger oxidative stress by impairing mitochondrial and lysosomal functions in neurons, as well as various other pathways, ultimately leading to neuronal damage.

Conclusions

The present study demonstrated that $Aβ_{25-35}$ could increase the concentration of $_iZn^{2+}$ by decreasing the expression levels of ZnT-3 and MT-3 mRNA in hippocampal neurons, eventually resulting in more serious neuronal death. Moreover, $Aβ_{25-35}$-induced $_iZn^{2+}$ increase significantly upregulated the expression level of Cav1.2 mRNA in hippocampal neurons, leading to increased L-I_{Ca} activities, resulting in increased neuronal excitability, thereby mediating $Aβ_{25-35}$-induced neuronal excitotoxic damage. Furthermore, the excessive $_iZn^{2+}$ induced by $Aβ_{25-35}$ synergistically increased $_iCa^{2+}$ in hippocampal neurons, leading to the damage of mitochondrial and lysosomal functions, resulting in an increase in ROS levels in neurons, thus mediating the neuronal damage by $Aβ_{25-35}$. These findings support the notion of a causal link between Aβ accumulation, $_iZn^{2+}$ and $_iCa^{2+}$ dyshomeostasis, and the dysregulation of crucial brain signaling molecules (Fig. 9). Whereas TPEN attenuated $Aβ_{25-35}$-induced neuronal damage by recovering the concentrations of $_iZn^{2+}$ and $_iCa^{2+}$ in neurons, decreasing L-I_{Ca} activity and intracellular ROS levels, reducing oxidative stress, and restoring mitochondrial and lysosomal functions. Therefore, maintaining $_iZn^{2+}$ homeostasis may be an effective way to alleviate Aβ-induced neuronal damage in AD. TPEN, a specific-free Zn^{2+} chelator, has been shown to be neuroprotective by counteracting the neurotoxicity of Aβ and may represent a potential cell-targeted therapy in Zn^{2+}-related diseases. However, our conclusions are somewhat limited due to the relatively simple and fixed assay conditions. To confirm these primary findings, more dose-dependent and in vivo experiments are required.

Data Availability The data that support the findings of this study are available from the corresponding author upon reasonable request.

Code Availability Not applicable.

Declarations

Ethics Approval and Consent to Participate All procedures were compliant with the approved protocol from the Animal Ethics Committee of Nankai University and the Chinese animal welfare act and the "Chinese code of practice and use of animals for scientific purposes."

Consent to Participate Not applicable.

Consent for Publication Not applicable.

Competing Interests The authors declare no competing interests.

References

1. Walsh DM, Selkoe DJ (2004) Deciphering the molecular basis of memory failure in Alzheimer's disease. Neuron 44(1):181–193. https://doi.org/10.1016/j.neuron.2004.09.010

2. Swerdlow RH (2007) Pathogenesis of Alzheimer's disease. Clin Interv Aging 2(3):347–359

3. Yamasaki T, Muranaka H, Kaseda Y, Mimori Y, Tobimatsu S (2012) Understanding the pathophysiology of Alzheimer's disease and mild cognitive impairment: a mini review on fMRI and ERP studies. Neurol Res Int 2012:719056. https://doi.org/10.1155/2012/719056

4. Minkeviciene R, Rheims S, Dobszay MB, Zilberter M, Hartikainen J, Fülöp L, Penke B, Zilberter Y et al (2009) Amyloid beta-induced neuronal hyperexcitability triggers progressive epilepsy. J Neurosci 29(11):3453–3462. https://doi.org/10.1523/jneurosci.5215-08,2009

5. Praticò D (2008) Oxidative stress hypothesis in Alzheimer's disease: a reappraisal. Trends Pharmacol Sci 29(12):609–615. https://doi.org/10.1016/j.tips.2008.09.001

6. Mucke L, Selkoe DJ (2012) Neurotoxicity of amyloid β-protein: synaptic and network dysfunction. Cold Spring Harb Perspect Med 2(7):a006338. https://doi.org/10.1101/cshperspect.a006338

7. Narayanan SE, Rehuman NA, Harilal S, Vincent A, Rajamma RG, Behl T, Uddin MS, Ashraf GM, Mathew B (2020) Molecular mechanism of zinc neurotoxicity in Alzheimer's disease. Environ Sci Pollut Res Int 27(35):43542–43552. https://doi.org/10.1007/s11356-020-10477-w

8. Tyszka-Czochara M, Grzywacz A, Gdula-Argasińska J, Librowski T, Wiliński B, Opoka W (2014) The role of zinc in the pathogenesis and treatment of central nervous system (CNS) diseases. Implications of zinc homeostasis for proper CNS function. Acta Pol Pharm 71(3):369–377

9. Tamano H, Oneta N, Shioya A, Adlard PA, Bush AI, Takeda A (2019) In vivo synaptic activity-independent co-uptakes of amyloid β(1–42) and Zn(2+) into dentate granule cells in the normal brain. Sci Rep 9(1):6498. https://doi.org/10.1038/s41598-019-43012-0

10. McCord MC, Aizenman E (2014) The role of intracellular zinc release in aging, oxidative stress, and Alzheimer's disease. Front Aging Neurosci 6:77. https://doi.org/10.3389/fnagi.2014.00077

11. Deibel MA, Ehmann WD, Markesbery WR (1996) Copper, iron, and zinc imbalances in severely degenerated brain regions in Alzheimer's disease: possible relation to oxidative stress. J Neurol Sci 143(1–2):137–142. https://doi.org/10.1016/s0022-510x(96)00203-1

12. Hane F, Leonenko Z (2014) Effect of metals on kinetic pathways of amyloid-β aggregation. Biomolecules 4(1):101–116. https://doi.org/10.3390/biom4010101

13. Deshpande A, Kawai H, Metherate R, Glabe CG, Busciglio J (2009) A role for synaptic zinc in activity-dependent Abeta oligomer formation and accumulation at excitatory synapses. J Neurosci 29(13):4004–4015. https://doi.org/10.1523/jneurosci.5980-08.2009

14. Berridge MJ (1998) Neuronal calcium signaling. Neuron 21(1):13–26. https://doi.org/10.1016/s0896-6273(00)80510-3

15. Supnet C, Bezprozvanny I (2010) The dysregulation of intracellular calcium in Alzheimer disease. Cell Calcium 47(2):183–189. https://doi.org/10.1016/j.ceca.2009.12.014

16. Popugaeva E, Chernyuk D, Bezprozvanny I (2020) Reversal of calcium dysregulation as potential approach for treating Alzheimer's disease. Curr Alzheimer Res 17(4):344–354. https://doi.org/10.2174/1567205017666200528162046

17. Popugaeva E, Pchitskaya E, Bezprozvanny I (2018) Dysregulation of intracellular calcium signaling in Alzheimer's disease. Antioxid Redox Signal 29(12):1176–1188. https://doi.org/10.1089/ars.2018.7506

18. Alzheimer's Association Calcium Hypothesis Workgroup (2017) Calcium hypothesis of Alzheimer's disease and brain aging: a framework for integrating new evidence into a comprehensive theory of pathogenesis. Alzheimer's Dement 13(2):178–182. https://doi.org/10.1016/j.jalz.2016.12.006

19. Jadiya P, Kolmetzky DW, Tomar D, Di Meco A, Lombardi AA, Lambert JP, Luongo TS, Ludtmann MH et al (2019) Impaired mitochondrial calcium efflux contributes to disease progression in models of Alzheimer's disease. Nat Commun 10(1):3885. https://doi.org/10.1038/s41467-019-11813-6

20. Foster TC, Kyritsopoulos C, Kumar A (2017) Central role for NMDA receptors in redox mediated impairment of synaptic function during aging and Alzheimer's disease. Behav Brain Res 322(Pt B):223–232. https://doi.org/10.1016/j.bbr.2016.05.012

21. Anekonda TS, Quinn JF, Harris C, Frahler K, Wadsworth TL, Woltjer RL (2011) L-type voltage-gated calcium channel blockade with isradipine as a therapeutic strategy for Alzheimer's disease. Neurobiol Dis 41(1):62–70. https://doi.org/10.1016/j.nbd.2010.08.020

22. Cai Q, Jeong YY (2020) Mitophagy in Alzheimer's disease and other age-related neurodegenerative diseases. Cells 9(1):150(1-28). https://doi.org/10.3390/cells9010150

23. Tang Y, Zucker RS (1997) Mitochondrial involvement in post-tetanic potentiation of synaptic transmission. Neuron 18(3):483–491. https://doi.org/10.1016/s0896-6273(00)81248-9

24. Kang JS, Tian JH, Pan PY, Zald P, Li C, Deng C, Sheng ZH (2008) Docking of axonal mitochondria by syntaphilin controls their mobility and affects short-term facilitation. Cell 132(1):137–148. https://doi.org/10.1016/j.cell.2007.11.024

25. Tönnies E, Trushina E (2017) Oxidative stress, synaptic dysfunction, and Alzheimer's disease. J Alzheimer's Dis JAD 57(4):1105–1121. https://doi.org/10.3233/jad-161088

26. Lin MT, Beal MF (2006) Mitochondrial dysfunction and oxidative stress in neurodegenerative diseases. Nature 443(7113):787–795. https://doi.org/10.1038/nature05292

27. Swerdlow RH, Burns JM, Khan SM (2010) The Alzheimer's disease mitochondrial cascade hypothesis. J Alzheimer's Dis JAD 20(Suppl 2):S265-279. https://doi.org/10.3233/jad-2010-100339

28. Swerdlow RH, Burns JM (1842) Khan SM (2014) The Alzheimer's disease mitochondrial cascade hypothesis: progress and

perspectives. Biochem Biophys Acta 8:1219–1231. https://doi.org/10.1016/j.bbadis.2013.09.010

29. Chen WB, Wang YX, Wang HG, An D, Sun D, Li P, Zhang T, Lu WG et al (2021) TPEN attenuates amyloid-β(25–35)-induced neuronal damage with changes in the electrophysiological properties of voltage-gated sodium and potassium channels. Mol Brain 14(1):124. https://doi.org/10.1186/s13041-021-00837-z

30. Livak KJ, Schmittgen TD (2001) Analysis of relative gene expression data using real-time quantitative PCR and the 2(-delta delta C(T)) method. Methods 25(4):402–408. https://doi.org/10.1006/meth.2001.1262

31. Tamano H, Nishio R, Shakushi Y, Sasaki M, Koike Y, Osawa M, Takeda A (2017) In vitro and in vivo physiology of low nanomolar concentrations of Zn^{2+} in artificial cerebrospinal fluid. Sci Rep 7:42897. https://doi.org/10.1038/srep42897

32. Frederickson CJ, Giblin LJ, Krezel A, McAdoo DJ, Mueller RN, Zeng Y, Balaji RV, Masalha R et al (2006) Concentrations of extracellular free zinc (pZn)e in the central nervous system during simple anesthetization, ischemia and reperfusion. Exp Neurol 198(2):285–293. https://doi.org/10.1016/j.expneurol.2005.08.030

33. Takeda A, Nakamura M, Fujii H, Tamano H (2013) Synaptic Zn^{2+} homeostasis and its significance. Metallomics 5(5):417–423. https://doi.org/10.1039/c3mt20269k

34. Krall RF, Tzounopoulos T, Aizenman E (2021) The function and regulation of zinc in the brain. Neuroscience 457:235–258. https://doi.org/10.1016/j.neuroscience.2021.01.010

35. Colvin RA, Bush AI, Volitakis I, Fontaine CP, Thomas D, Kikuchi K, Holmes WR (2008) Insights into Zn^{2+} homeostasis in neurons from experimental and modeling studies. Am J Physiol Cell Physiol 294(3):C726-742. https://doi.org/10.1152/ajpcell.00541.2007

36. Shuttleworth CW, Weiss JH (2011) Zinc: new clues to diverse roles in brain ischemia. Trends Pharmacol Sci 32(8):480–486. https://doi.org/10.1016/j.tips.2011.04.001

37. Takeda A, Tamano H, Tempaku M, Sasaki M, Uematsu C, Sato S, Kanazawa H, Datki ZL et al (2017) Extracellular Zn^{2+} is essential for amyloid $β_{1-42}$-induced cognitive decline in the normal brain and its rescue. J Neurosci 37(30):7253–7262. https://doi.org/10.1523/jneurosci.0954-17.2017

38. Takeda A, Koike Y, Osaw M, Tamano H (2018) Characteristic of extracellular Zn^{2+} influx in the middle-aged dentate gyrus and its involvement in attenuation of LTP. Mol Neurobiol 55(3):2185–2195. https://doi.org/10.1007/s12035-017-0472-z

39. Solomonov I, Korkotian E, Born B, Feldman Y, Bitler A, Rahimi F, Li H, Bitan G, Sagi I (2012) Zn^{2+}-$Aβ_{40}$ complexes form metastable quasi-spherical oligomers that are cytotoxic to cultured hippocampal neurons. J Biol Chem 287(24):20555–20564. https://doi.org/10.1074/jbc.M112.344036

40. Ji SG, Medvedeva YV, Wang HL, Yin HZ, Weiss JH (2019) Mitochondrial Zn^{2+} accumulation: a potential trigger of hippocampal ischemic injury. Neuroscientist 25(2):126–138. https://doi.org/10.1177/1073858418772548

41. Forostyak O, Forostyak S, Kortus S, Sykova E, Verkhratsky A, Dayanithi G (2016) Physiology of Ca^{2+} signalling in stem cells of different origins and differentiation stages. Cell Calcium 59(2–3):57–66. https://doi.org/10.1016/j.ceca.2016.02.001

42. Colbourne F, Grooms SY, Zukin RS, Buchan AM, Bennett MV (2003) Hypothermia rescues hippocampal CA1 neurons and attenuates down-regulation of the AMPA receptor GluR2 subunit after forebrain ischemia. Proc Natl Acad Sci USA 100(5):2906–2910. https://doi.org/10.1073/pnas.2628027100

43. Stork CJ, Li YV (2009) Rising zinc: a significant cause of ischemic neuronal death in the CA1 region of rat hippocampus. J Cereb Blood Flow Metab 29(8):1399–1408. https://doi.org/10.1038/jcbfm.2009.64

44. Chasapis CT, Loutsidou AC, Spiliopoulou CA, Stefanidou ME (2012) Zinc and human health: an update. Arch Toxicol 86(4):521–534. https://doi.org/10.1007/s00204-011-0775-1

45. Baltaci AK, Yuce K (2018) Zinc transporter proteins. Neurochem Res 43(3):517–530. https://doi.org/10.1007/s11064-017-2454-y

46. Baltaci AK, Yuce K, Mogulkoc R (2018) Zinc metabolism and metallothioneins. Biol Trace Elem Res 183(1):22–31. https://doi.org/10.1007/s12011-017-1119-7

47. Yu WH, Lukiw WJ, Bergeron C, Niznik HB, Fraser PE (2001) Metallothionein III is reduced in Alzheimer's disease. Brain Res 894(1):37–45. https://doi.org/10.1016/s0006-8993(00)03196-6

48. Beyer N, Coulson DT, Heggarty S, Ravid R, Irvine GB, Hellemans J, Johnston JA (2009) ZnT3 mRNA levels are reduced in Alzheimer's disease post-mortem brain. Mol Neurodegener 4:53. https://doi.org/10.1186/1750-1326-4-53

49. Lee SJ, Koh JY (2010) Roles of zinc and metallothionein-3 in oxidative stress-induced lysosomal dysfunction, cell death, and autophagy in neurons and astrocytes. Molecular brain 3(1):30. https://doi.org/10.1186/1756-6606-3-30

50. Calvo-Rodriguez M, Bacskai BJ (2021) Mitochondria and calcium in Alzheimer's disease: from cell signaling to neuronal cell death. Trends Neurosci 44(2):136–151. https://doi.org/10.1016/j.tins.2020.10.004

51. Arispe N, Rojas E, Pollard HB (1993) Alzheimer disease amyloid beta protein forms calcium channels in bilayer membranes: blockade by tromethamine and aluminum. Proc Natl Acad Sci USA 90(2):567–571. https://doi.org/10.1073/pnas.90.2.567

52. Ferreiro E, Oliveira CR, Pereira C (2004) Involvement of endoplasmic reticulum Ca^{2+} release through ryanodine and inositol 1,4,5-triphosphate receptors in the neurotoxic effects induced by the amyloid-beta peptide. J Neurosci Res 76(6):872–880. https://doi.org/10.1002/jnr.20135

53. Wang R, Reddy PH (2017) Role of glutamate and NMDA receptors in Alzheimer's disease. J Alzheimer's Dis JAD 57(4):1041–1048. https://doi.org/10.3233/jad-160763

54. Navakkode S, Liu C, Soong TW (2018) Altered function of neuronal L-type calcium channels in ageing and neuroinflammation: Implications in age-related synaptic dysfunction and cognitive decline. Ageing Res Rev 42:86–99. https://doi.org/10.1016/j.arr.2018.01.001

55. Berger SM, Bartsch D (2014) The role of L-type voltage-gated calcium channels Cav1.2 and Cav1.3 in normal and pathological brain function. Cell Tissue Res 357(2):463–476. https://doi.org/10.1007/s00441-014-1936-3

56. Ritz B, Rhodes SL, Qian L, Schernhammer E, Olsen JH, Friis S (2010) L-type calcium channel blockers and Parkinson disease in Denmark. Ann Neurol 67(5):600–606. https://doi.org/10.1002/ana.21937

57. Webster NJ, Ramsden M, Boyle JP, Pearson HA, Peers C (2006) Amyloid peptides mediate hypoxic increase of L-type Ca^{2+} channels in central neurones. Neurobiol Aging 27(3):439–445. https://doi.org/10.1016/j.neurobiolaging.2005.02.002

58. Hotka M, Cagalinec M, Hilber K, Hool L, Boehm S, Kubista H (2020) L-type $Ca(2+)$ channel-mediated $Ca(2+)$ influx adjusts neuronal mitochondrial function to physiological and pathophysiological conditions. Sci Signal 13(618):eaaw6923(1-15). https://doi.org/10.1126/scisignal.aaw6923

59. Forette F, Seux ML, Staessen JA, Thijs L, Babarskiene MR, Babeanu S, Bossini A, Fagard R et al (2002) The prevention of dementia with antihypertensive treatment: new evidence from the Systolic Hypertension in Europe (Syst-Eur) study. Arch Int Med 162(18):2046–2052. https://doi.org/10.1001/archinte.162.18.2046

60. Pannicke T, Iandiev I, Uckermann O, Biedermann B, Kutzera F, Wiedemann P, Wolburg H, Reichenbach A et al (2004) A potassium channel-linked mechanism of glial cell swelling in the

postischemic retina. Mol Cell Neurosci 26(4):493–502. https://doi.org/10.1016/j.mcn.2004.04.005

61. Jaffe DB, Ross WN, Lisman JE, Lasser-Ross N, Miyakawa H, Johnston D (1994) A model for dendritic Ca^{2+} accumulation in hippocampal pyramidal neurons based on fluorescence imaging measurements. J Neurophysiol 71(3):1065–1077. https://doi.org/10.1152/jn.1994.71.3.1065

62. Schulien AJ, Justice JA, Di Maio R, Wills ZP, Shah NH, Aizenman E (2016) Zn2+-induced Ca2+ release via ryanodine receptors triggers calcineurin-dependent redistribution of cortical neuronal Kv2.1 K+ channels. J Physiol 594(10):2647–2659. https://doi.org/10.1113/jp272117

63. Wallace DC (2005) A mitochondrial paradigm of metabolic and degenerative diseases, aging, and cancer: a dawn for evolutionary medicine. Ann Rev Genet 39:359–407. https://doi.org/10.1146/annurev.genet.39.110304.095751

64. Malaiyandi LM, Vergun O, Dineley KE, Reynolds IJ (2005) Direct visualization of mitochondrial zinc accumulation reveals uniporter-dependent and -independent transport mechanisms. J Neurochem 93(5):1242–1250. https://doi.org/10.1111/j.1471-4159.2005.03116.x

65. Sensi SL, Paoletti P, Bush AI, Sekler I (2009) Zinc in the physiology and pathology of the CNS. Nat Rev Neurosci 10(11):780–791. https://doi.org/10.1038/nrn2734

66. Abramov AY, Canevari L, Duchen MR (2004) Calcium signals induced by amyloid beta peptide and their consequences in neurons and astrocytes in culture. Biochem Biophys Acta 1742(1–3):81–87. https://doi.org/10.1016/j.bbamcr.2004.09.006

67. Angelova PR, Abramov AY (2014) Interaction of neurons and astrocytes underlies the mechanism of Aβ-induced neurotoxicity. Biochem Soc Trans 42(5):1286–1290. https://doi.org/10.1042/bst20140153

68 Görlach A, Bertram K, Hudecova S, Krizanova O (2015) Calcium and ROS: a mutual interplay. Redox Biol 6:260–271. https://doi.org/10.1016/j.redox.2015.08.010

69. Colacurcio DJ, Nixon RA (2016) Disorders of lysosomal acidification-the emerging role of v-ATPase in aging and neurodegenerative disease. Ageing Res Rev 32:75–88. https://doi.org/10.1016/j.arr.2016.05.004

70. Seo BR, Lee SJ, Cho KS, Yoon YH, Koh JY (2015) The zinc ionophore clioquinol reverses autophagy arrest in chloroquine-treated ARPE-19 cells and in APP/mutant presenilin-1-transfected Chinese hamster ovary cells. Neurobiol Aging 36(12):3228–3238. https://doi.org/10.1016/j.neurobiolaging.2015.09.006

71. Zheng L, Kågedal K, Dehvari N, Benedikz E, Cowburn R, Marcusson J, Terman A (2009) Oxidative stress induces macroautophagy of amyloid beta-protein and ensuing apoptosis. Free Radical Biol Med 46(3):422–429. https://doi.org/10.1016/j.freeradbiomed.2008.10.043